Elastic, optical and thermodynamic properties of the double perovskites Ba_2DySbO_6: Applications in spintronic devices

S. Ilhem Messaoudi and A. Touia*.

Faculty of Sciences and Technology, University of Ain Temouchent, Belhadj Bouchaib. BP 284, Ain-Temouchent, 46000,
**e-mail: amina.touia@univ-temouchent.edu.dz*

Received 17 November 2025; accepted 2 April 2026

In this research, we employed an ab initio calculation approach based on the full-potential linearized augmented plane wave (FP-LAPW) method within the framework of density functional theory (DFT), integrated into the WIEN2k code. By examining in detail the structural, elastic, electronic, magnetic, optical, and thermodynamic characteristics of the double perovskite compound Ba_2DySbO_6. Firstly, our study focused primarily on magnetic stability. The results presented in this work are in good agreement with the available experimental and theoretical data. Subsequently, we studied the electronic properties in which we calculated the band structure and the density of states. Regarding the magnetic properties of the compound Ba_2DySbO_6, it was found that the total magnetic moment is mainly due to the magnetic moment of the lanthanide atom. The optical properties, such as the real and imaginary parts of the dielectric function, the refractive index, the extinction coefficient, the reflectivity, the optical conductivity, and the absorption coefficient of the Ba_2DySbO_6 compound, were calculated for all photon energies. The thermodynamic study of our compound has shown that it is stable at high temperatures. The predictive calculations of the thermal properties of our compound show that it follows the same behavior with temperature variation.

Keywords: Elastic; optical; thermodynamic; DFT, Ba_2DySbO_6.

DOI: https://doi.org/10.31349/RevMexFis.72.051601

1. Introduction

In recent years, double perovskites have gained enormous interest and have become one of the most motivating subjects in the field of scientific research due to the extraordinary physical and electrical properties that characterize this family of compounds. Some of the double perovskites with the general formula $A_2B'B''O_6$ (where A is generally an alkaline earth or rare earth metal, B' and B" are transition metals or lanthanides) have been proposed as ferroelectric, such as Ba_2GdMoO_6 [1]. Furthermore, it has been well known that these compounds possess particular characteristics of interest among them; their structural and physical properties are very sensitive to small changes in chemical composition. Therefore, depending on the choice of cations A, B', and B", they can exhibit a wide variety of crystalline structures, including structures with monoclinic ($P2_1/n$), tetragonal (I4/m), and cubic ($Fm\bar{3}m$) symmetries [2, 3], as well as electrical and magnetic properties that include metallicity and magnetoelectric response [4]. Perovskite compounds with the basic structure Ba_2RESbO_6, (where RE = Nd, Eu, and Dy), were prepared as single-phase materials using standard solid-state methods. These compounds are isostructural and exhibit a complex perovskite structure, as shown by powder X-ray diffraction measurements [5–7]. Ab initio simulation studies, within the framework of DFT, have been dedicated to this promising class of double perovskite oxides containing magnetic ions in B' sites. But, despite these recent advances in understanding the physical properties of these compounds, several other questions regarding electronic, magnetic, elastic, optical, and thermodynamic structures are still debatable. For these reasons, in this work, we performed first-principles calculations based on the full-potential linearized augmented plane wave (FP-LAPW) method, implemented in the Wien2k code, with the generalized gradient approximation (GGA-PBE) of the double perovskite compound Ba_2DySbO_6.

2. Computational details

By examining in detail the structural, elastic, electronic, magnetic, optical, and thermodynamic properties of the double perovskite compound Ba_2DySbO_6, we were able to obtain useful information for this compound using methods based on DFT [8, 9] with the generalized gradient approximation (GGA-PBE) [10–12]. Within the framework of these studies, the application of DFT generally begins with total energy calculations and structural optimization steps. Therefore, in this work, we studied the cubic double perovskite Ba_2DySbO_6. This compound crystallizes in the space group (No. 225) described by $a = b = c$ and $\alpha = \beta = \gamma = 90°$. The positions of the Ba, Dy, Sb, and O atoms, respectively, are Ba (0.25, 0.25, 0.25), Ba (0.75, 0.75, 0.75), Dy (0.0, 0.0, 0.0), Sb (0.5, 0.5, 0.5), and O (u=0.2851, 0, 0) [7]. The cubic structure of Ba_2DySbO_6 is illustrated in Fig. 1. The Wien2k program, which is directly based on the application of the FP-LAPW method [13] allows for the calculation of various properties, such as the total energy. This code uses DFT-based techniques and considers both the space group symmetry and the Bravais lattice. The exchange-correlation functional was described using the GGA-PBE approximation [10]. The value

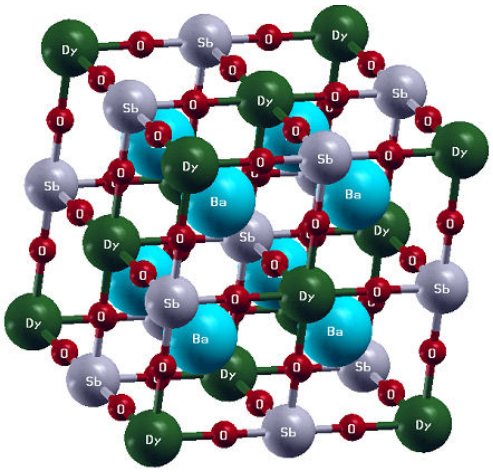

FIGURE 1. Crystal structure of double perovskites Ba_2DySbO_6.

of $\ell_{\max} = 10$ defines the cutoff used to determine the angular momentum of the functions inside the sphere. The parameter $G_{\max} = 14$ indicates the largest wave vector norm (K) used to carry out the Fourier (plane-wave) expansion of the charge density. The cutoff parameter $R_{\mathrm{MT}} \times K_{\max}$=8 determines the basis functions to be used in the calculation, where RMT is the smallest radius of the Muffin-tin (MT) spheres in the unit cell, and $K_{\max}$ is the norm of the largest wave vector (K) associated with the plane-wave expansion of the eigenfunctions. These parameters proved suitable for achieving convergence with an energy tolerance of 10^{-4} Ry and the cut-off energy between the valence states and the core states was set at -6 eV. The integration in reciprocal space is performed with a mesh of $14 \times 14 \times 14$, resulting in 3000 k-points in the irreducible Brillouin zone (IBZ) [14]. The radii of the MT spheres (RMT) of the Ba, Dy, Sb, and O atoms chosen in our calculations are respectively, 2.5, 2.25, 1.98, and 1.7 a.u. (atomic unit). To verify the crystal structures of double perovskites, the tolerance factor was calculated using the expression $t = (r_A + r_0)/(\sqrt{2}(r_B + r_0))$. The Shannon ionic radii of Ba^{2+}, Dy^{3+}, Sb^{5+}, and O^{2-} were used to determine the tolerance factor t of the four cations: 1.61 Å (Ba^{2+}), 0.912 Å (Dy^{3+}), 0.6 Å (Sb^{5+}), and 1.4 Å (O^{2-}). The average radius of Dy and Sb was used for the B site to give an average B-cation radius of 0.756 Å and a tolerance factor of about $t \approx 0.99$, indicating that the B-site cations have a stable configuration in a cubic structure. Depending on the value of the tolerance factor, the structure of double perovskites is cubic since t is between 0.9-1 [15].

3. Results and discussion

3.1. Structural and elestic properties

The calculation of the physical properties of double perovskites requires the determination of their ground state. To achieve this, we evaluated the total energy of the system for different volume values. In order to determine the magnetic stability (ferromagnetic and non-magnetic configurations) and structural properties (lattice parameter a, compressibility modulus B, and its derivative B') in the vicinity of equilibrium, we analyzed the energy differences and structural responses for each configuration. The obtained results were then fitted by the third-order Birch-Murnaghan equation of state [16]. Figure 2 represents the variation of total energy as a function of volume for both the magnetic and non-magnetic phases, using the GGA-PBE approximation with and without spin polarization. The results obtained regarding the ground state energy and structural parameters such as, the lattice parameter, the bulk modulus B, and its derivative B', are compiled in Table I, along with the experimental values and those obtained by other theoretical calculations for comparison. The most stable ferromagnetic state is identified because it corresponds to the phase with the minimum energy. The results presented in Table I above are in good agreement with the available experimental and theoretical data [6, 17–22]. Comparing these data in percentage, we find a slight overestimation of the lattice parameters cal-

TABLE I. Lattice constant a_0 (in Å), bulk modulus B (in GPa), its pressure derivative B', and minimum energy at equilibrium E_0 (in Ryd) using GGA (PBE).

Method / Work	$\mathbf{a_0}$ **(Å)**	**B (GPa)**	$\mathbf{B'}$	$\mathbf{E_0}$ **(Ry)**
NM-GGA-PBE	8.7097	105.1572	5.3211	-70738.804736
FM-GGA-PBE	8.5372	129.2429	4.8769	-70765.738955
Experimental	8.431 [6]	-	-	-
	8.4247 [17]	-	-	-
	8.4289 [18]	-	-	-
	8.4374 [18]	-	-	-
	8.4247 [20]	-	-	-
	8.4297 [21]	-	-	-
	8.4376 [22]	-	-	-
Theoretical	8.4243 [19]	-	-	-

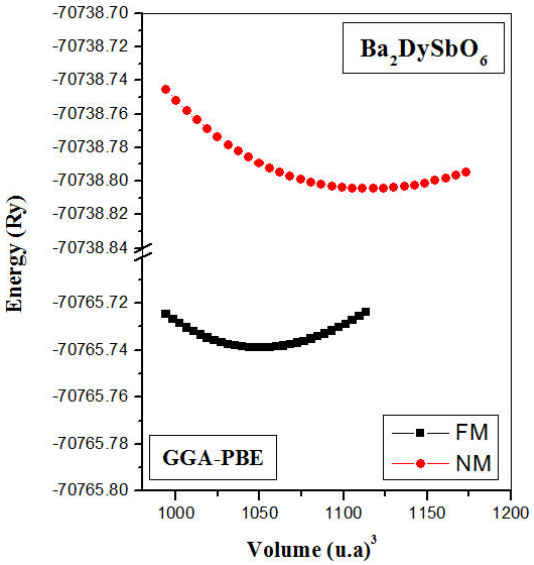

FIGURE 2. The total energy for both non-magnetic (NM) and ferromagnetic (FM) configurations with the GGA (PBE) approximation as a function of volume.

TABLE II. Calculated elastic constants C_{11}, C_{12}, C_{44} (in GPa), bulk modulus B (in GPa), Young's modulus E and shear modulus G (in GPa), Poisson's ratio ν, the anisotropic parameter A and the B/G ratio, longitudinal, transverse and average sound velocities (v_l, v_t, v_m) (in $\mathrm{m\,s^{-1}}$), and Debye temperature θ_D (in K) calculated using GGA (PBE) at $T = 0$ K and $P = 0$ GPa.

Elastic constants (GPa)			
C_{11}	C_{12}	C_{44}	$B = \frac{C_{11}+2C_{12}}{3}$
211.8	98.7	80.7	136.36
Mechanical properties			
E (GPa)	G (GPa)	ν	A	B/G
181.5861	71.04	0.28	1.42	1.92
Sound velocities ($\mathrm{m\,s^{-1}}$) and Debye temperature			
v_l	v_t	v_m	θ_D (K)
3182.955	5740.639	3545.581	195.2865

culated by the GGA (PBE) approximation on the order of: 3.32% and 1.26% for the non-magnetic and ferromagnetic states, respectively, due to the use of GGA(PBE).

To determine the elastic properties of the Ba_2DySbO_6 compound, we first applied orthorhombic and monoclinic constraints, respectively. The requirement of mechanical stability of the cubic structure leads to the following restrictions on the elastic constants, $C_{11} > 0$, $C_{12} > 0$, $C_{44} > 0$, and $(C_{11} + 2C_{12}) > 0$ [23, 24]. Our obtained elastic constants listed in Table II, obey these stability conditions for cubic structures, including the fact that $C_{12} > 0$ must be less than $C_{11} > 0$. Furthermore, our calculated elastic constants also meet the stability conditions for cubic structures, which implies that $C_{12} < B < C_{11}$. The value of the bulk modulus B, calculated from the elastic constants, is nearly the same as the value obtained from the smoothing points $E_{\mathrm{tot}}(V)$ using the Murnaghan equation of state (EOS). This gives us a good estimate of the precision and accuracy of the elastic constants of Ba_2DySbO_6. The calculated value of A, which is listed in Table II, indicates that Ba_2DySbO_6 is a material exhibiting anisotropic behavior (if $A \neq 1$, indicates anisotropic behavior, while A = 1 corresponds to isotropic behavior). The typical value of the Poisson coefficient for covalent materials is around 0.1, while for ionic materials it is around 0.25 [23, 24]. In our case, the value of the Poisson's ratio is 0.28, which suggests a stronger intra-atomic ionic bonding contribution for this compound. According to Pugh's empirical formula [23, 24], which states that the critical value of the B/G ratio separating the ductile and brittle behavior of materials is approximately 1.75, *i.e.*, if $B/G > 1.75$, the material behaves in a ductile manner; otherwise, it behaves in a brittle manner, the Ba_2DySbO_6 compound is classified as ductile.

3.2. Electronic and magnetic properties

The band structure calculation of the double perovskite Ba_2DySbO_6 was performed along the high-symmetry directions of the first Brillouin zone [25] based on the GGA-PBE approximation. The results obtained are illustrated in Fig. 3 for both spin-up and spin-down. According to these figures, it is evident that the band structure of minority spins (spin-down) has a spin polarization around the Fermi level, which indicates that this electronic structure has a purely metallic character, while the majority spins (spin-up) exhibit a semiconducting behavior, with the maximum and minimum of the valence band and conduction band located at the Γ point, indicating the presence of a direct band gap in the $(\Gamma - \Gamma)$ direction for the Ba_2DySbO_6 material, which confirms that this compound is typically ferromagnetic semi-metallic by GGA-PBE. The energy gap value, from the spin-up band structure diagram, is equal to 3.19 eV for the Ba_2DySbO_6 compound. In our study, we calculated the density of states (DOS) of this material Ba_2DySbO_6. Figure 4 shows the partial density of

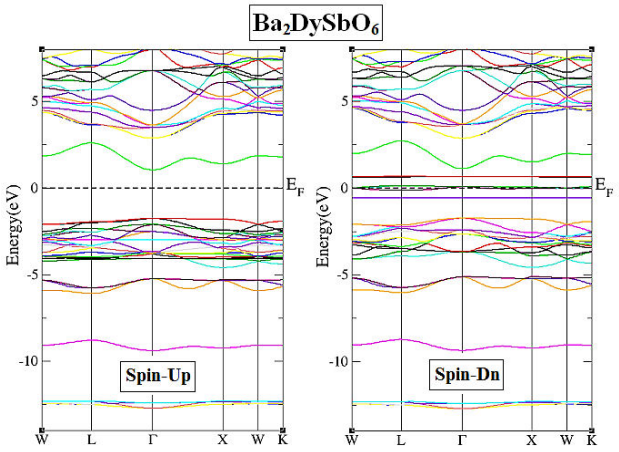

FIGURE 3. The band structure of Ba_2DySbO_6 at the equilibrium structure using PBE-GGA approximation with spin polarization.

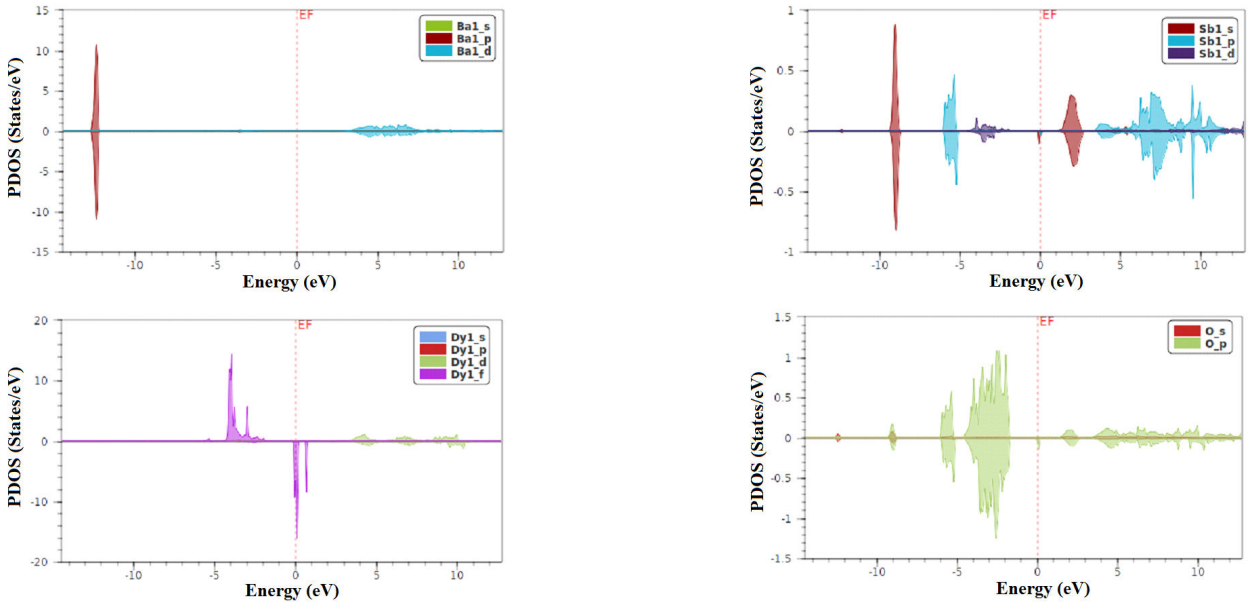

FIGURE 4. The partial density of states of Ba_2DySbO_6 at the equilibrium structure using PBE-GGA approximation with spin polarization.

TABLE III. Total and local magnetic moments of Ba_2DySbO_6 obtained by the GGA-PBE approximation, with spin polarization.

Method	Ba	Dy	Sb	O	Interstitial	Total
GGA-PBE (at $T = 0$ K)	-0.00047	4.86657	-0.00731	0.01815	0.03000	5.0
Theoretical (at $T \neq 0$ K)	–	–	–	–	–	7.7 [7]
Experimental (at $T \neq 0$ K)	–	–	–	–	–	8.9 [7]
	–	–	–	–	–	10.55 [21]
	–	–	–	–	–	10.63 [21]

states (PDOS) calculated using the generalized gradient approach (GGA-PBE) with spin polarization between -13 and 15 eV relative to the Fermi level. We observe for this compound Ba_2DySbO_6 below the Fermi level, the valence band is strongly dominated by Ba-p (up and down) and Dy-f (up) states with, however, a minor contribution from Sb-s,p and O-p (up and down) states around the Fermi level, the states are dominated by Dy-f (down) orbitals. Above the Fermi level (states located about 1 eV and higher), in the conduction band, the PDOS is weakly dominated by Sb-p (up and down) and O-p (up and down) states. We also note that the partial density of states (PDOS) calculated using (GGA-PBE) with spin polarization of this Ba_2DySbO_6 compound for both spin-up and spin-down cases are not similar, which confirms that the material is magnetic. The results presented in Figs. 3 and 4 are in good agreement with the available theoretical data [7, 19]. We calculated the total, partial, and interstitial magnetic moments of the double perovskite compound Ba_2DySbO_6 using the GGA-PBE approximation and with spin polarization. According to Table III, the compound Ba_2DySbO_6 has a significant total magnetic moment, indicating the presence of ferromagnetic behavior in this material in its ground state. We also notice that the total contributions are much more localized on the lanthanide atom Dy. The experimental and theoretical data are represented in Table III. The difference in total magnetic moments is due to the change in temperature ($T \neq 0$ K).

3.3. Optical properties

The GGA-PBE approximation was adopted to study the optical properties of the Ba_2DySbO_6 compound. In this section, optical properties such as the real and imaginary parts of the dielectric function, reflectivity, refractive index, extinction coefficient, optical conductivity, and absorption coefficient of the Ba_2DySbO_6 compound were calculated for all photon energy, and they are presented in Figs. 5-10 respectively. In Fig. 5, the fixed value of the real part $\varepsilon_1(0)$, which relates to the material's interaction with low-frequency, is quite high, suggesting a strong polarization capacity. $\varepsilon_1(\omega)$ peaks at about 0.67 eV, indicating a strong coupling of the material to the incoming photons in this energy range. After this point, $\varepsilon_1(\omega)$ decreases and becomes negative at about 1.01 eV, showing that the material enters a metallic reflection phase. The disappearance of $\varepsilon_1(\omega)$ signifies the presence of a bulk plasmon, which is a collective excitation of conduction electrons. The real part $\varepsilon_1(\omega)$ starts very high (ranging from approximately 25 to 30), then decreases with increasing

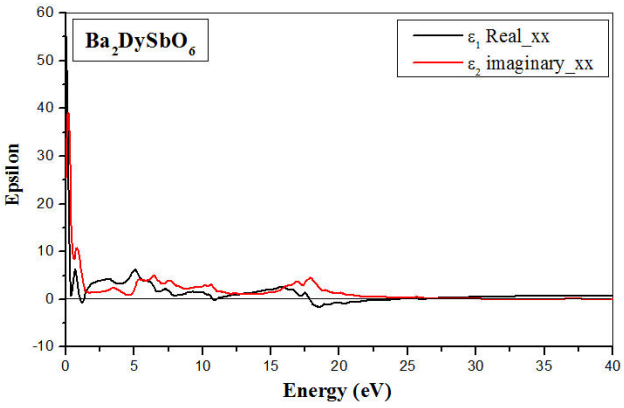

FIGURE 5. The real part $\varepsilon_1(\omega)$ and imaginary part $\varepsilon_2(\omega)$ of dielectric function of Ba_2DySbO_6 compound.

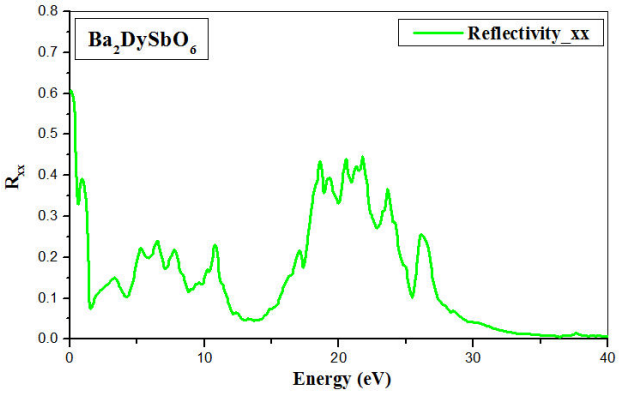

FIGURE 6. The reflectivity $R(\omega)$ of Ba_2DySbO_6 compound.

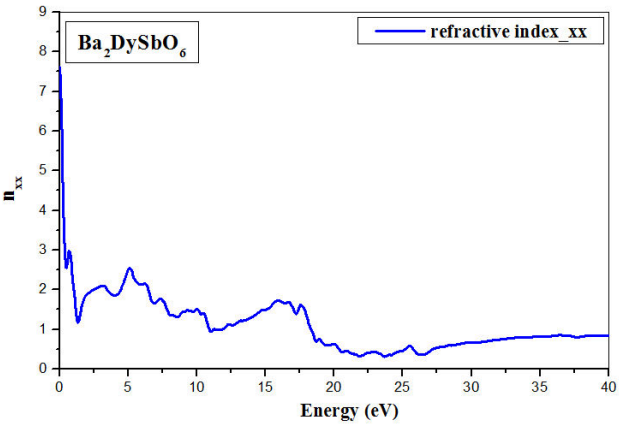

FIGURE 7. The refractive index $n(\omega)$ of Ba_2DySbO_6 compound.

energy, eventually crossing zero at approximately 16 to 17 eV, indicating the presence of a plasmon resonance. The imaginary part $\varepsilon_2(\omega)$ can be directly linked to the material's optical absorption, indicating electronic transitions between the bands. A distinct peak is observed at 0.16 eV, which is ascribed to electronic transitions into the upper conduction bands. For energy values larger than 0.18 eV, $\varepsilon_2(\omega)$ gradually decreases indicating that the absorption decreases as interband transitions become less available. The intermediate energy region has multiple smaller peaks (around 4 to 5) at approximately 5 eV, (around 2 to 3) at approximately 10 eV, and (around 3 to 4) between 16 and 18 eV, which correspond to multiple electronic transitions related to the band gap energy. Above 22 eV, both $\varepsilon_1(\omega)$ and $\varepsilon_2(\omega)$ tend to zero, and the material approaches transparency. Overall, there is strong interaction between the material and light in the low and intermediate energy ranges. Figure 6 illustrates the evolution of reflectivity R according to photon energy for the material Ba_2DySbO_6. Reflectivity is a crucial factor for evaluating the proportion of light reflected by the material's surface during electromagnetic excitation and is directly related to the refractive index and extinction coefficient. We observe a low reflectivity value at energies $E < 3\,\mathrm{eV}$, indicating a high degree of absorption or transmission by the material of most of the incident illumination, followed by a significant increase from $3\,\mathrm{eV}$ onward, still with oscillations that most often coincide with the peaks we observe earlier in the extinction coefficient. The region beyond $30\,\mathrm{eV}$ shows a stabilized reflectivity value; the slight oscillations observed could be due to plasmonic effects and secondary electronic transitions. The Ba_2DySbO_6 material refractive index (n) evolution is illustrated in Fig. 7, as a function of photon energy, progressively increasing from 0.51 eV before reaching maximal n around 3 at a photon energy of 0.70 eV. The enhancement of refractive index (n) is due to the contribution of inter-band electron transitions that increase the optical response of the material, and refractive index (n) begins to decrease slightly after $17.67\,\mathrm{eV}$ due to related absorption increasing as more electrons are excited into higher energy levels. Starting from $25\,\mathrm{eV}$, the refractive index (n) becomes really low, which means the materials are not effectively transmitting light in this spectral region. Analyzing the refractive index is very useful to understand the optical properties of the material and its different utilizations, especially in optoelectronics and photonics, where a high refractive index is desirable to serve as a waveguide for some wavelength ranges, for nonlinear optical devices, or even for antireflective applications. Therefore, the analysis of this curve provides a better understanding of the light-electron interaction mechanism in Ba_2DySbO_6 and thus progresses its potential applications. It appears from Fig. 8 that a significant peak around $0.24\,\mathrm{eV}$ is observed in the extinction coefficient of about 0.45, indicating strong optical absorption resulting from allowed electronic transitions. These transitions are determined by the band structure of the solid, which can also cause several secondary peaks that reflect other modes of electronic transitions. In Fig. 9, we represent the variation of optical conductivity (σ_x) as a function of energy for the material Ba_2DySbO_6, whose appearance is characterized by a very significant peak located in the vicinity of $17.92\,\mathrm{eV}$, which could correspond to a strong absorption of incident photons due to dominant inter-band electronic transitions. We indeed observe that after this peak, the conductivity decreases with some oscillation, with secondary electronic transitions and

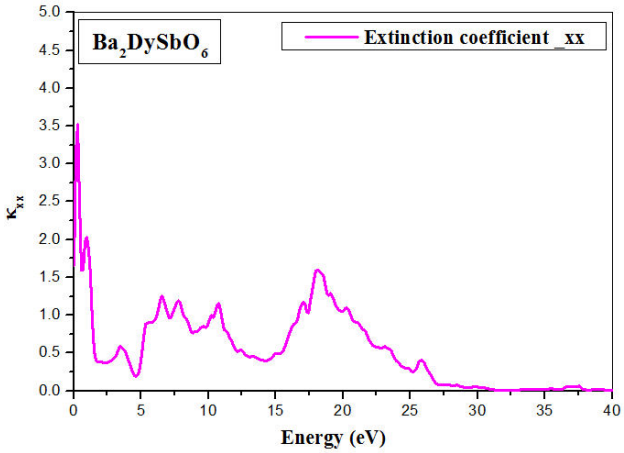

FIGURE 8. The extinction coefficient $k(\omega)$ of Ba_2DySbO_6 compound.

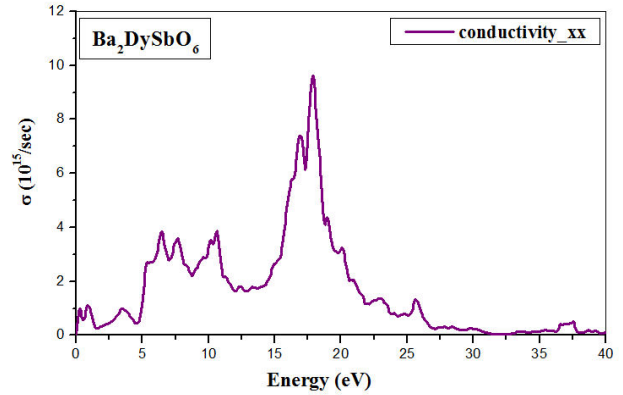

FIGURE 9. The conductivity $\sigma(\omega)$ of Ba_2DySbO_6 compound.

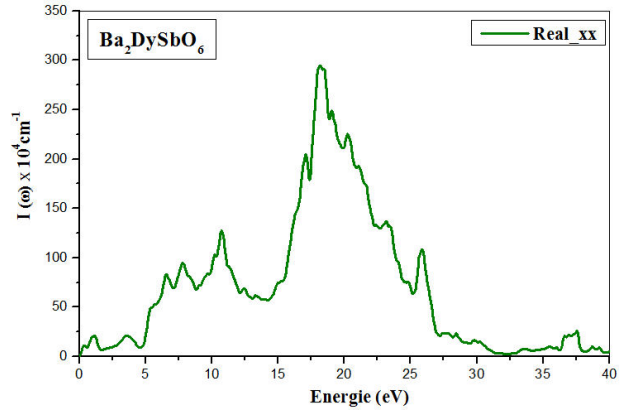

FIGURE 10. The absorption $I(\omega)$ of Ba_2DySbO_6 compound.

density of states effects opposing the main transition. Figure 10 shows the evolution of the absorption coefficient of the Ba_2DySbO_6 material as a function of the energy of the incident photons. Optical absorption is indeed an important parameter for understanding the electronic and optical properties of a material, both for optoelectronic and photovoltaic applications, and here, the absorption coefficient gradually increases until it reaches a maximum around $18.17\,\mathrm{eV}$, then decreases. This trend is generally observed for materials undergoing inter-band transitions between the valence and the conduction band, where the absorption peak is related to direct electronic transitions.

3.4. Thermodynamic properties

To address the thermodynamic properties of the double perovskite compound Ba_2DySbO_6, we apply the quasi-harmonic Debye model to the GIBBS program [11, 14, 26]. This model allows the extraction of all thermodynamic properties from the energy and volume properties, provided at equilibrium. To study the thermal properties of the double perovskite compound Ba_2DySbO_6 at high temperature and high pressure, we applied the quasi-harmonic Debye approximation. To begin, a calculation of the total energy as a function of the unit volume $E(V)$, was performed and associated with the numerical equation of state (EOS) to determine the structural parameters at room temperature and zero pressure, and to deduce the macroscopic properties as a function of pressure and temperature from classical thermodynamic relations. The thermal properties are calculated over the temperature range of $0-700\,\mathrm{K}$ using the GGA-PBE method, where the quasi-harmonic model is fully valid. In Fig. 11, the curve of the lattice parameter is shown as a function of temperature and for different pressures for the double perovskite compound Ba_2DySbO_6. The lattice parameter increases with increasing temperature, but the percentage increase is more significant for the temperature range above $150\,\mathrm{K}$. On the other hand, when the pressure (P) increases (from 0 to $40\,\mathrm{GPa}$), the lattice parameter decreases at a given temperature (from 0 to $700\,\mathrm{K}$). The graph plotted in Fig. 12 illustrates the variation of the compressibility modulus (B) with temperature at the considered pressure. It appears that, (from 0 to $150\,\mathrm{K}$), the compressibility modulus is almost constant, while at high temperatures $(T > 150\,\mathrm{K})$, a linear decrease is observed with increasing temperature. At a given pressure, the compressibility increases with temperature, and at a given temperature, it increases as the pressure decreases. At the temperature

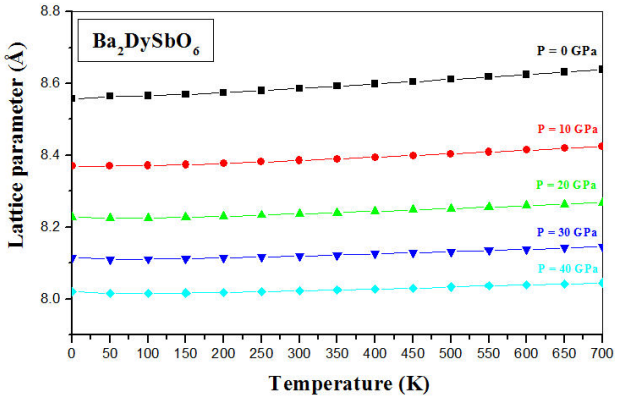

FIGURE 11. The variation of lattice parameter as a function of temperature of Ba_2DySbO_6: at different pressures.

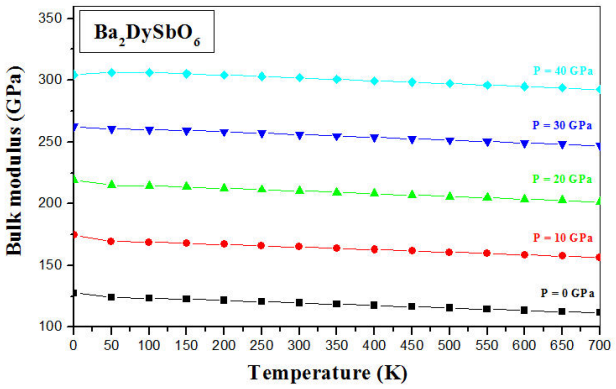

FIGURE 12. The variation of bulk modulus B as a function of temperature for Ba_2DySbO_6: at different pressures.

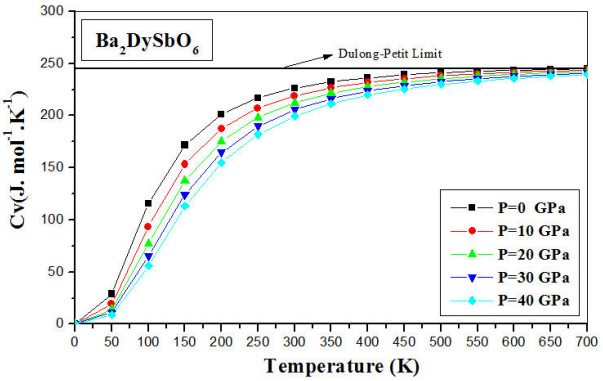

FIGURE 13. The variation of heat capacity C_v as a function of temperature for Ba_2DySbO_6: at different pressures.

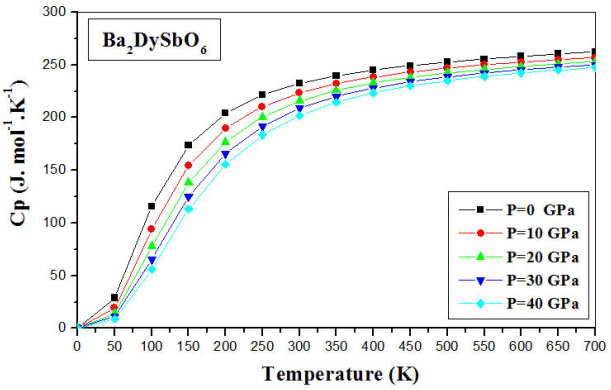

FIGURE 14. The variation of heat capacity C_p as a function of temperature for Ba_2DySbO_6: at different pressures.

$T = 0\,\mathrm{K}$ and $P = 0\,\mathrm{GPa}$, the modulus $B = 127.6789\,\mathrm{GPa}$. At elevated temperatures, the specific heat (or heat capacity at constant volume C_v) changes only slightly with temperature and approaches the Dulong-Petit limit [11, 14, 26], which all solids attain at high temperature in the limit. The variation of the heat capacity C_v as a function of temperature at pressures ranging from 0–40 GPa is shown in Fig. 13. We then observe that for $T < 300\,\mathrm{K}$, the heat capacity C_v increases rapidly with temperature. At higher temperatures ($T > 300\,\mathrm{K}$), C_v

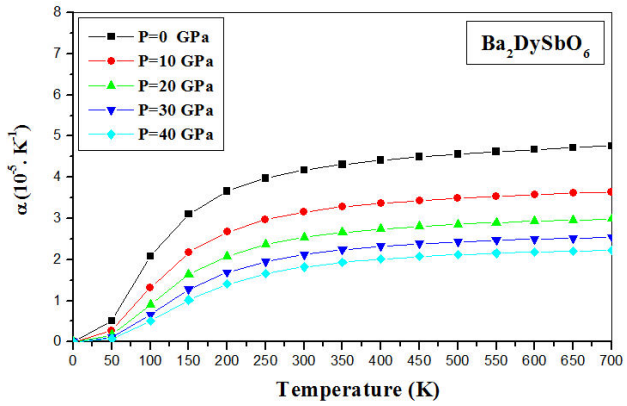

FIGURE 15. The variation of thermal expansion coefficient α as a function of temperature for Ba_2DySbO_6: at different pressures.

approaches the Dulong-Petit limit, as is common for most solid materials at high temperatures. At high temperature, it reaches a value of $245.2951\,\mathrm{J\,mol^{-1}\,K^{-1}}$. Figure 14 shows how C_p varies with temperature under different pressures for the double perovskite based on Ba_2DySbO_6. The variation of C_p with temperature is comparable to that of C_v at low temperatures; at high temperatures, C_p is different from C_v which becomes constant. The effect of pressure on the heat capacity at constant pressure C_p is substantially identical to that of C_v. Figure 15 illustrates the effect of temperature on the thermal expansion coefficient (α), which increases with temperature. At a given pressure, the thermal coefficient (α) increases quite significantly with temperature up to $300\,\mathrm{K}$, beyond which α becomes progressively more linear with temperature. At $P = 0\,\mathrm{GPa}$ and $T = 300\,\mathrm{K}$, the thermal expansion coefficient α is found to be $4.17409 \times 10^{-5}\,\mathrm{K^{-1}}$. Entropy (S) could be defined as a measure of the disorder of a system at the microscopic level. When the entropy of the system decreases, its constituents become more ordered, bound, and capable of producing mechanical effects. The increase in temperature can easily be translated into an increase in disorder as measured by entropy, as evidenced by the increase in possible positions of the molecules. Figure 16 shows the variation of entropy (S) as a function of temperature and pressure for the double perovskite Ba_2DySbO_6.

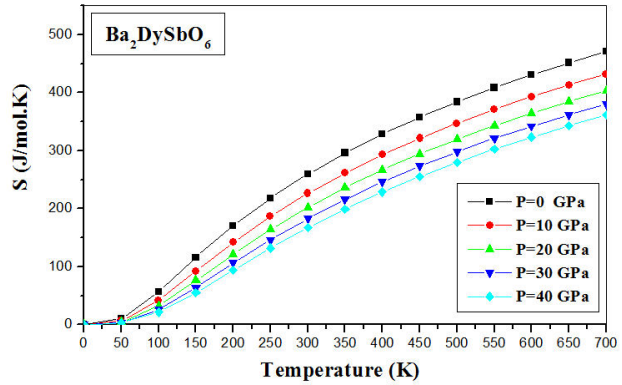

FIGURE 16. The variation of entropy as a function of temperature for Ba_2DySbO_6: at different pressures.

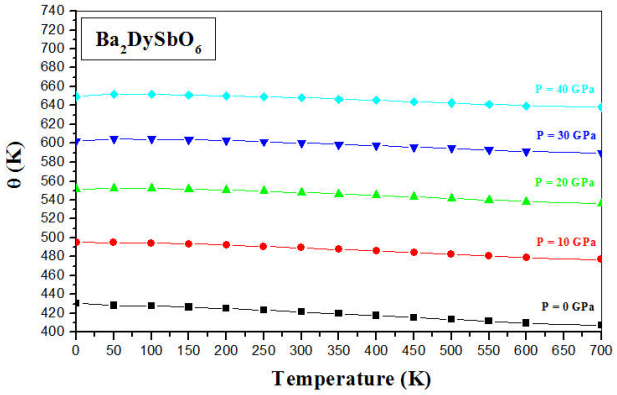

FIGURE 17. The variation of Debye temperature as a function of temperature for Ba_2DySbO_6: at different pressures.

For a given pressure, it is observed that the entropy (S) has a strong temperature dependence (which increases very rapidly with increasing temperature), but conversely, the entropy (S) decreases at a given temperature with increasing pressure. Heating favors the vibrational contribution to entropy, therefore, the entropy (S) increases with temperature. In Fig. 17, the Debye temperatures θ^D are represented as a function of temperature for several pressure values. It appears that θ^D remains constant from $0-40\,\mathrm{K}$, then decreases linearly with increasing temperature. At a fixed temperature, the Debye temperature increases with the rise in pressure. By superimposing this curve with Fig. 12, related to the compressibility modulus, we note that θ^D and (B) follow the same evolution. Due to the type of approximation chosen, there is a non-negligible difference between the Debye temperatures θ^D obtained by the elastic method $(\theta^D = 195.2865\,\mathrm{K})$ and the thermodynamic method $(\theta^D = 430.6\,\mathrm{K})$, at $T = 0\,\mathrm{K}$ and $P = 0\,\mathrm{GPa}$. Indeed, only low-frequency acoustic modes are taken into account by the elastic approach, thus leading to an underestimation of the Debye temperature; whereas the thermodynamic approach pays attention to the entire photon spectrum by including optical modes, thus providing a higher and therefore more representative estimate of the Debye temperature for the material's behavior. The Debye temperature cannot be considered a unique quantity but only as a function of the evaluation method adopted.

4. Conclusion

In the present study, we used an ab initio method based on the full-potential linearized augmented plane wave (FP-LAPW) method within the framework of density functional theory (DFT). The method focused on the structural, elastic, electronic, magnetic, and thermodynamic properties of the Ba_2DySbO_6 compound in its GGA-PBE version. After studying the magnetic stability, we found that the ferromagnetic state is the most stable configuration, because it is associated with the phase that has the lowest total energy. The results of the present study are in good agreement with the experimental and theoretical data found in the literature. The elastic constants obtained meet the stability conditions; the calculated value of the factor (A) indicates that Ba_2DySbO_6 is an anisotropic material. In our case, the Poisson's ratio value of 0.28 means that the intra-atomic ionic bonding contribution would be higher for this compound. From our results, the material displays semi-metallic characteristics with a direct $(\Gamma - \Gamma)$ gap in the spin-up channel while the spin-down channel remains metallic. Thus, spin polarization is quite evident at the Fermi level in both channels, making it a unique property for spintronic applications. Consequently, Ba_2DySbO_6 may be a suitable candidate for spintronic devices such as spin filters, spin injectors, and magnetic tunnel junctions in which the performance is determined by a spin-dependent transport property. The compound Ba_2DySbO_6 demonstrates in the partial density of states (PDOS) calculated with (GGA-PBE) that the valence band, below the Fermi level, is strongly dominated by Ba-p (up and down) and Dy-f (up) states, while around the Fermi level, the states are dominated by Dy-f (down). Above the Fermi level, the PDOS in the conduction band is weakly dominated by Sb-s and Sb-p (up-down) states. Regarding the magnetic properties of the compound Ba_2DySbO_6, we have shown that the total magnetic moment is primarily due to the magnetic moment of the lanthanide atom Dy. The results of the density of states and band structure show that the compound has a semi-metallic character and is a good candidate for spintronic applications. According to the calculations of optical properties, this material exhibits high sensitivity in the energy region between visible light and extreme ultraviolet (UV). Materials with broad peaks in the UV range are used in various fields such as disinfection, spectroscopy, and printing. Finally, the thermodynamic parameters such as the heat capacity at constant volume (C_V), the heat capacity (C_p) at constant pressure, the thermal expansion coefficient (α), the Debye temperature (θ^D), and the entropy (S) of our product Ba_2DySbO_6 were determined and discussed. Next, the effect of pressure on the lattice parameter and the compressibility modulus (B) was also studied. All things considered, the thermodynamic properties of our Ba_2DySbO_6 material are good and efficient.

Declarations conflict of interest

The authors declare no competing financial interest.

Data availability statement

The data that support the findings of this study are available from the corresponding author upon reasonable request.

1. T. K. Wallace, R. H. Colman, and A. C. McLaughlin, Variable temperature synchrotron X-ray diffraction study of the ferroelastic double perovskite Ba_2GdMoO_6, *Phys. Chem. Chem. Phys.* **15** (2013) 8672-8677, https://doi.org/10.1039/C2CP43732E.
2. A. K. Azad, S. G. Eriksson, S. A. Ivanov, H. Rundlöf, J. Eriksen, R. Mathieu, and P. Svedlindh, Structural and magnetic characterisation of the double perovskites $AA'MnWO_6$ ($AA' = Ba_2$, SrBa, Sr_2, SrCa, Ca_2), *Ferroelectrics* **269** (2002) 105-110, https://doi.org/10.1080/00150190211167.
3. R. P. Borges *et al*., Magnetic properties of the double perovskites A_2FeMoO_6: A = Ca, Sr, Ba, *J. Phys.: Condens. Matter* **11** (1999) L445, https://doi.org/10.1088/0953-8984/11/40/104.
4. V. R. Palkar and S. K. Malik, Observation of magnetoelectric behavior at room temperature $Pb(Fe_xTi_{1-x})O_3$, *Solid State Commun.* **134** (2005) 783-786, https://doi.org/10.1016/j.ssc.2005.01.032.
5. P. R. S. Wariar, J. Kurian, P. K. Sajith, T. G. N. Babu, and J. Koshy, Ba_2RESbO_6 (RE = Nd, Eu and Dy); Characterization and potential use as substrate for superconducting YBCO films, *Mod. Phys. Lett. B* **11** (1997) 889-897, https://doi.org/10.1142/S0217984997001092.
6. P. García Casado, A. Mendiola, and I. Rasines, On the Perovskites Ba_2LnSbO_6 (Ln = Nd, Sm, Eu, Gd, Tb, Dy, Ho, Er, Yb), *Z. Anorg. Allg. Chem*. **510** (1984) 194-198, https://doi.org/10.1002/zaac.19845100327.
7. R. Cardona, R. Moreno-Mendoza, L. A. Carrero-Bermúdez, D. A. Landínez-Téllez, and J. Roa-Rojas, Crystalline, magnetic and electronic structure of the Ba_2DySbO_6 complex perovskite, *J. Low Temp. Phys*. **182** (2016) 61-71, https://doi.org/10.1007/s10909-015-1353-3.
8. A. Ababou *et al*., DFT-based computer simulation of the physical properties of transparent conducting oxide of delafossite-type: $AgInO_2$ and $AgYO_2$, *Physica B: Condens. Matter* **601** (2021) 412584, https://doi.org/10.1016/j.physb.2020.412584.
9. A. Touia, K. Benyahia, and A. Tekin, First-principles calculations of structural, electronic, optical, and thermoelectric properties of LuNiBi and LuNiSb half-Heusler, *J. Supercond. Nov. Magn*. **34** (2021) 2689-2698, https://doi.org/10.1007/s10948-021-05970-3.
10. J. P. Perdew, M. Ernzerhof, and K. Burke, Rationale for mixing exact exchange with density functional approximations, *J. Chem. Phys.* **105** (1996) 9982-9985, https://doi.org/10.1063/1.472933.
11. S. I. Messaoudi, A. Touia, and O. Addou, Optoelectronic and thermodynamic properties of the yttrium filled skutterudite YFe_4P_{12}, *Rev. Mex. Fís.* **70** (2024) 061601, https://doi.org/10.31349/RevMexFis.70.061601.
12. M. Fodil, A. Touia, S. Bousalem, O. Baraka, and A. Mokadem, Thermoelectric, optoelectronic, and magnetic properties of Pb_2CoWO_6 double perovskite in the cubic phase: using DFT+U via spin-orbit coupling, *Indian J. Phys.* **98** (2024) 3901-3911, https://doi.org/10.1007/s12648-024-03154-y.
13. P. Blaha, K. Schwarz, G. K. H. Madsen, D. Kvasnicka, and J. Luitz, WIEN2k: An augmented plane wave + local orbitals program for calculating crystal properties, *Comput. Phys. Commun.* **60** (2001) 155-169, https://doi.org/10.1007/s10909-015-1353-3.
14. A. Touia, M. Benkhaled, C. Khobzaoui, and M. Fodil, Optical and thermodynamic properties of half-Heusler compound TaIrSn: using modified Becke-Johnson (mBJ), *J. Supercond. Nov. Magn.* **34** (2021) 2865-2877, https://doi.org/10.1007/s10948-021-05981-0.
15. S. A. Mir *et al*., Structural and elasto-mechanical properties of ordered double perovskite Ba_2LuSbO_6, *AIP Conf. Proc*. (2019), https://doi.org/10.1063/1.5113176.
16. F. Birch, Finite elastic strain of cubic crystals, *Phys. Rev*. **71** (1947) 809, https://doi.org/10.1103/PhysRev.71.809.
17. A. Majid, M. F. Ahmad, and T. S. Choi, Lattice constant prediction of $A_2BB'O_6$ type double perovskites, in: *Proc. Int. Conf. Comput. Sci. Its Appl*. (2009), https://doi.org/10.1007/978-3-642-02457-3_7.
18. Y. M. Jana, S. Nandi, A. A. Biswas, H. C. Gupta, R. Upadhyay, C. Upadhyay, and D. Samanta, Optical and magnetic properties of cubic double perovskites Ba_2RSbO_6 (R = Dy, Gd) coordinated to lattice dynamical and crystal-field computations, *Phys. Status Solidi B* **259** (2022) 2100460, https://doi.org/10.1002/pssb.202100460.
19. D. K. Jha *et al*., Ab initio study of double perovskites Ba_2DySbO_6, AIP Conf. Proc. (2016), https://doi.org/10.1063/1.4948000.
20. H. Karunadasa, Q. Huang, B. G. Ueland, P. Schiffer, and R. J. Cava, Ba_2LnSbO_6 and Sr_2LnSbO_6 (Ln = Dy, Ho, Gd) double perovskites: Lanthanides in the geometrically frustrating fcc lattice, *Proc. Natl. Acad. Sci. U.S.A.* **100** (2003) 8097-8102, https://doi.org/10.1073/pnas.0832394100.
21. S. Otsuka and Y. Hinatsu, Structures and magnetic properties of rare earth double perovskites containing antimony or bismuth Ba_2LnMO_6 (Ln = rare earths; M = Sb, Bi), *J. Solid State Chem*. **227** (2015) 132-141, https://doi.org/10.1016/j.jssc.2015.03.034.
22. C. Vijayakumar *et al*., Synthesis, characterization and dielectric properties of nanocrystalline Ba_2DySbO_6 perovskite, *J. Alloys Compd*. **475** (2009) 778-781, https://doi.org/10.1016/j.jallcom.2008.08.013.
23. A. Touia, C. Khobzaoui, M. Benkhaled, and M. Fodil, Structural, elastic, electronic, and magnetic properties of XPtBi (X = Er and Ho) using FP-LAPW method, *J. Supercond. Nov. Magn*. **34** (2021) 1865-1873, https://doi.org/10.1007/s10948-021-05888-w.
24. A. Touia, M. Ameri, and I. Ameri, Synthesis, crystal structure and physical properties of the thulium filled skutterudite $TmFe_4P_{12}$ under the effect of pressure: LDA and LSDA calculation, *Optik* **126** (2015) 3253-3259, https://doi.org/10.1016/j.ijleo.2015.07.130.
25. O. Addou, K. Benyahia, and A. Touia, Synthesis, structural, electronic, magnetic, optical and thermoelectric properties of XPd_2Bi (X = Tb, Dy, Ho) for spintronics devices, *Braz. J. Phys.* (2023), https://doi.org/10.1007/s13538-023-01339-0.

26. A. Touia, K. Benyahia, I. S. Messaoudi, and A. Tekin, Comparative study of structural, electronic, magnetic and thermodynamic properties of $TbInZ_2$ (Z = Cu, Ag, and Au), *Acta Phys. Pol. A* (2022), https://doi.org/10.12693/APhysPolA.141.210.